Reactivity of a gas/metal/metal-oxide three-phase boundary: CO oxidation at the Pt(1 1 1)–c(4 × 2)-2CO/α-PtO₂ phase boundary

W.X. Li [a], B. Hammer [b,*]

[a] Center for Theoretical and Computational Chemistry, Dalian Institute of Chemical Physics, Chinese Academy of Sciences, 116023 Dalian, China
[b] Interdisciplinary Nanoscience Center (iNANO) and Department of Physics and Astronomy, University of Aarhus, DK-8000 Aarhus C, Denmark

Abstract

We present a density functional theory study of a chemical reaction at a three-phase boundary. The three phases are the gas phase of the reactants and products, an adsorbate covered metallic catalyst surface phase, and an oxidized catalyst surface phase. Specifically, the CO oxidation reaction is investigated at the Pt(1 1 1)–c(4 × 2)-2CO/α-PtO₂ phase boundary. A number of different structural phase boundary models are considered, and in every case we find special reaction sites showing smaller energy barriers than inside a reference Pt(1 1 1)–p(2 × 2)-(O + CO) coadsorption structure. Our results underline the importance of three-phase boundaries in heterogeneous catalysis.
© 2005 Elsevier B.V. All rights reserved.

1. Introduction

In recent years, much focus has been on closing the pressure and material gaps often present in surface science studies of catalytic surfaces. The application of in situ experimental techniques, including high-pressure scanning tunneling microscopy [1,2], X-ray diffraction [3], sum frequency generation [4,5], and high resolution transmission electron microscopy [6] have shown that catalytic surfaces often undergo structural transitions under reaction conditions. In the case of oxidation reactions at transition metal surfaces it has been suggested that high coverage oxygen chemisorption phases, surface oxide phases, or bulk oxide phases are the relevant reaction states of the surfaces. For Ru it has been demonstrated that with O₂ pressures above 10^{-2} mbar at 700 K the active state of the surface is the rutile RuO₂ [7], and for Pt(1 1 0) indications are that a Pt-oxide forms

under CO₂ production at O₂ pressures above 0.5 bar at 425 K [2].

The degree to which a catalytic metal surface oxidizes under reaction conditions is determined not only by thermodynamic but also by kinetic factors [8]. For a surface with a thermodynamic preference for undergoing oxidation, a slow surface oxidation kinetics might hinder this and result in steady-state conditions where surface oxygen is consumed in the catalyzed reaction rather than building up as a surface or bulk oxide. Kinetically driven oscillations in the surface state and reactivity under constant external pressure of the reactants might even occur as a consequence of several steady-state conditions being possible [9]. Clearly, at most one (if any) of the surface states involved in such oscillations can represent the thermodynamic equilibrium state, while the other must be a non-equilibrium state. This illustrates that non-equilibrium situations are encountered in catalysis and that several phases of the catalyst may coexist. The simplest such multi-phase situation would be that of the catalyst surface exposing both metallic and oxidized patches. In this case, three phases of matter converge in one region of space: the gas phase of the reactants and

products, the metallic, and the oxidized phases of the catalyst.

In the present work we show with density functional theory, that such three-phase boundaries constitute particularly reactive environments. The oxidation of CO by O_2 is chosen as the reaction and metallic and oxidized Pt are chosen as the catalysts. We find that the CO binds much more strongly to the metallic Pt than does oxygen. Consequently, we conduct our calculations with a high-coverage CO structure on the metallic Pt. The reaction of this CO with lattice O in the oxidized part of the catalyst is studied subsequently. Considering a number of different metal/metal-oxide phase boundary structures, we find that the CO oxidation can take place with a barrier which is smaller than in the reference configuration inside a Pt(1 1 1)–$p(2 \times 2)$-(O + CO) coadsorption structure. The reduced barriers at the gas/metal/metal-oxide three-phase boundaries are shown to result despite of stronger total adsorption of the reactants. This points to the availability of new, favorable transition states at the special phase boundary sites as the cause for the enhanced reactivity.

2. Method

The density functional theory calculations are performed using the slab and ultra soft pseudopotential approach for the ionic systems and a plane wave expansion ($E_{cut} = 25$ Ry) for the one-electron wave functions. The energetics discussed is based on the generalized gradient approximation (GGA) exchange-correlation (XC) functional in the revised Perdew, Burke, Ernzerhof (RPBE) form [10]. We further give, in one figure and some tables, non-self-consistent Perdew–Wang-1991 (PW91) [11] based energies. The theoretical lattice constant, 4.02 Å for fcc-Pt, surface unit cells of $(2\sqrt{3} \times 5)$ or $(2\sqrt{3} \times 6)$ size, and slabs of three frozen (1 1 1) layers were used. The effect of including another Pt layer (i.e. having four Pt layers) was found to be minor; oxygen differential adsorption potential energies within the oxide changed from -1.35 and -1.09 eV to -1.37 and -1.06 eV, respectively, while CO differential adsorption potential energies at the metal surface changed from -1.45, -1.08, and -1.07 eV to -1.37, -1.00, and -1.03 eV, respectively. Surface Brillouin zone sampling was done with **k**-point densities $\geqslant 7$ Å^2. Energy barriers were found by constrained relaxation [12,13]. With this method, a reaction pathway is assumed and configuration 'images' along the pathway are relaxed in all degrees of freedom except the reaction coordinate. Care is taken that, when adding more images, the pathways become continuous in the entire configuration space. The transition state (TS) is determined as the image of highest potential energy. To make the TS search computationally tractable,

we determined first, for each reaction system considered, the TS reaction coordinate value with images of two-layer Pt slabs. One image with a three-layer Pt slab was relaxed subsequently for each reaction system while keeping the reaction coordinate fixed. The resulting potential energy was used for evaluating the potential energy barrier.

3. Structure of three-phase boundary

Catalytical CO oxidation at Pt surfaces under non-equilibrium conditions has been investigated intensively. Examples include: (i) exposure of an oxygen pre-covered Pt(1 1 1) surface to CO [14,15], (ii) exposure of a CO pre-covered Pt(1 1 1) surface to high pressure O_2 [16], and (iii) time-dependent reactivity studies of Pt(1 1 0) under large and small CO/O_2 pressure ratios [2]. In case (i), the surface was found to accommodate two coexisting adsorbate phases, $c(4 \times 2)$-2CO, and $p(2 \times 2)$-(O + CO), in case (ii) vacancies in the saturated CO adsorption phase were found to be necessary during transient reaction conditions, and in case (iii), an oxide phase was shown to be growing during steady state reaction conditions. In the absence of CO, the completion of an oxide phase on Pt(1 1 0) has recently been found to be kinetically hindered [17] in line with the situation described at the Rh(1 1 1) surface [18]. A Pt surface exposed to a CO- and oxygen-gas mixture can thus be expected to exhibit both a chemisorbing, metallic phase and an oxidized phase, and three-phase boundaries may thus exist for this system.

As a starting point, we set up reliable models of three-phase boundaries taking into consideration the perimeter of Pt-oxide islands atop a Pt metal surface. The close-packed Pt(1 1 1) surface is chosen as it is expected to be most abundant on single crystal Pt particles. Platinum forms two oxides of comparable stability: a CdI$_2$-type α-PtO$_2$ [19] and a rutile-like CaCl$_2$-type β-PtO$_2$ [20]. The formation of Pt-oxide islands or overlayers is corroborated by the large O uptake over Pt(1 1 1) after exposure to ozone [21], by detection with X-ray photoelectron spectroscopy of an oxidic oxygen state after exposure of Pt(1 1 1) to atomic O [22], and by Fourier transformed infrared and X-ray absorption near-edge structure spectroscopy investigations of a model catalyst [23]. Recent surface X-ray diffraction results from the Frenken group further indicate that the α-PtO$_2$ forms over the Pt(1 1 1) [24] and we hence chose this structure for the oxide phase. The α-PtO$_2$ is composed of (0 0 0 1)-sheets of octahedrally oxygen-coordinated Pt. In the bulk structure, the sheets interact with weak van der Waals forces and hence the α-PtO$_2$(0 0 0 1) surface energy must be small and this facet abundant. In the present work we therefore compose the oxide island of one such layer, expecting thicker islands to have

similar behavior. Separate calculations show that the α-PtO$_2$(0001) surface is non-reactive in itself [25].

Fig. 1 shows the realization of the gas/metal/metal-oxide three-phase boundary in our calculations. For the oxide layer we chose two different relative Pt(111)/α-PtO$_2$(0001) positions. The PtO$_2$ sheet is parallel to the Pt(111) surface, either (A) with every third Pt atom
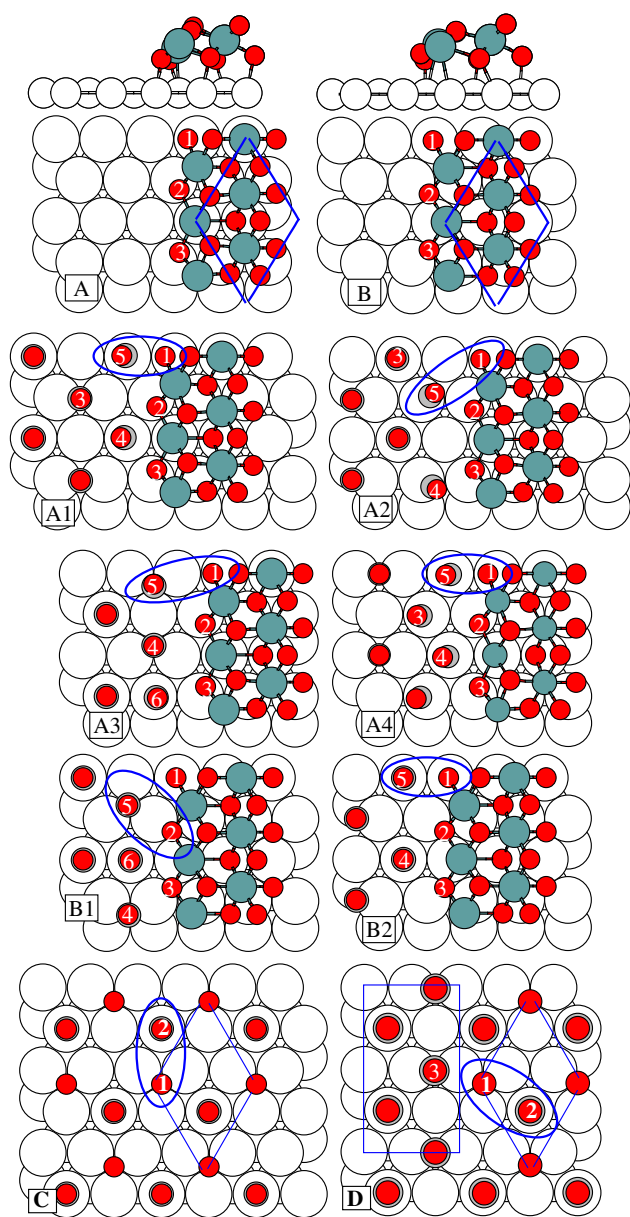

Fig. 1. A and B represent two possible realizations of the metal/metal-oxide phase boundary before CO adsorption on the metal part. A1, A2, A3, A4, B1 and B2 show structures after saturation of the metal part with CO. C and D depict the reaction inside $p(2\times2)$-(O + CO) and right at the boundary for one possible $c(4\times2)$-2CO/$p(2\times2)$-(O + CO) phase boundary. The reactants involved in the most favorable reaction paths are indicated. CO molecules labeled 4, 5, or 6 were fully relaxed as were the Pt and O atoms right inside the oxide edge.

in the oxide being atop a Pt atom in the Pt(111) or (B) with every sixth O atom in the oxide being atop a Pt atom in the Pt(111). The two different registries differ by only 0.04 eV per Pt(111)–(2 × 2) unit cell. The oxide sheet is cut along a [$1\bar{1}00$] direction that preserves five-fold O coordination of every edge Pt atom in the oxide. A small commensurable cell of the α-PtO$_2$(0001) and the Pt(111) is then obtained by aligning the oxide edge direction along the Pt[$\bar{2}10$] direction, straining the oxide slightly; the calculated equilibrium (in-plane) lattice constant of α-PtO$_2$ is 3.20 Å, while in our model it is expanded by 2.6% in the island-edge direction and allowed to relax perpendicular to the island-edge. The differential oxygen adsorption potential energies in the oxide phase are (numerically) high, −1.35, −1.10, and −1.09 eV in model A and −1.38, −0.83, and −0.91 eV in model B for O(1), O(2) and O(3), respectively. No further oxygen can be adsorbed at this edge. The metal-oxide layer is slightly over-stoichiometric in oxygen, Pt$_6$O$_{15}$ per cell, but the O-binding energies are representative of a stoichiometric oxygen layer. With a larger, stoichiometric Pt$_9$O$_{18}$ oxide layer the differential oxygen adsorption potential at, e.g., sites O(1) and O(3) of model A become −1.30 and −1.08 eV, respectively, i.e. within 50 meV of the results with the chosen model.

The introduction of chemisorbed oxygen on the metallic part of the Pt(111) exposed in the system would lead to an energy gain of the order 0.22 eV per surface Pt atom at 0.25 ML oxygen coverage. CO adsorption, on the other hand, releases about 1.46 eV per CO or 0.73 eV per surface Pt atom when a $c(4\times2)$-2CO overlayer is formed. Assuming not too different CO and O$_2$ partial pressures, it is thus likely that the metallic Pt phase will be CO covered. A more quantitative argument why the metallic part of the surface is expected to be CO rather than O covered is presented in Fig. 2. Here, the (restricted) equilibrium phase diagram [26] for Pt(111) in the presence of gaseous CO and O$_2$ is presented as a function of the chemical potential of the two gases.

Before interpreting Fig. 2, we would like to draw attention to Reuter, Frenkel and Scheffler's recent studies of CO oxidation at rutile RuO$_2$(110) using first-principles-based statistical mechanics [8]. These studies illustrate how, at specific conditions, kinetic restrictions may cause phases to appear, other than those predicted by equilibrium thermodynamics. In our case, we have already assumed that the growth of an oxide will be controlled by kinetics. We expect, however, the adsorption of either molecular CO or atomic O at the metallic part of the Pt surface to be less proned to be controlled by kinetics since, for instance, no Pt rearrangement is involved in the growth of such phases.

With the above considerations in mind, the GGA-RPBE based Fig. 2a suggests that for ambient partial pressures at room temperature (and even higher), the $c(4\times2)$-2CO overlayer forms on the metallic part of
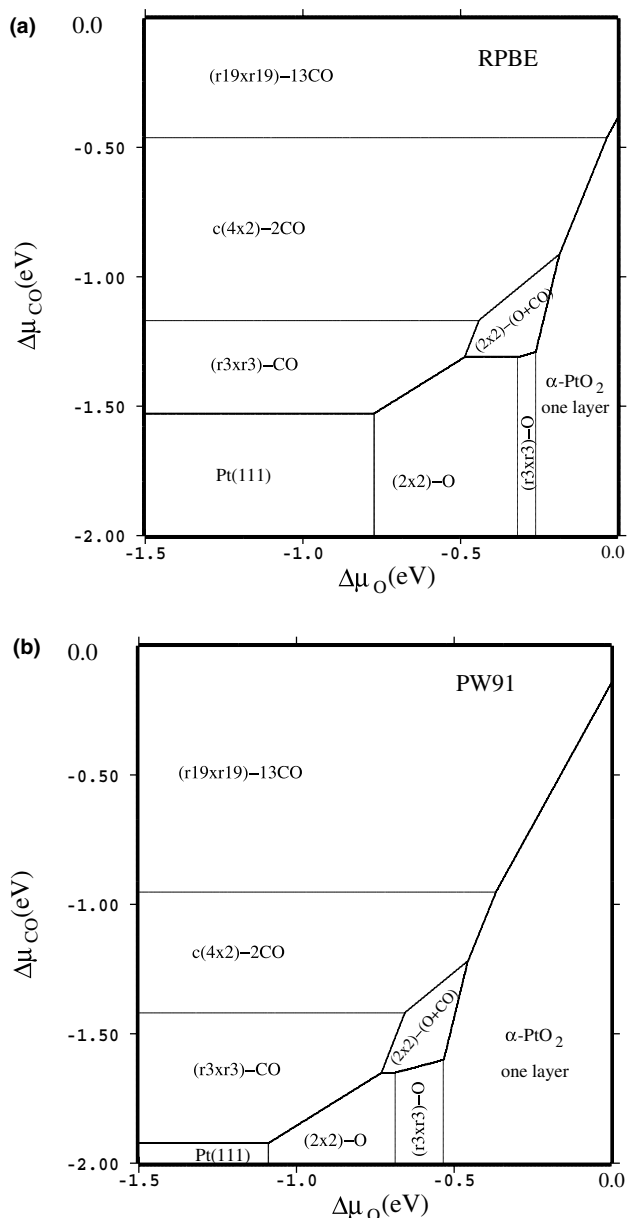
(a)

(b)

Fig. 2. Phase diagram for oxygen and CO coadsorption at Pt(111) calculated either within (a) GGA-RPBE or (b) GGA-PW91. Three pure CO phases, two pure O phases, one CO + O co-adsorption phase and one single (tri)-layer oxide structure were considered. 'r3' and 'r19' mean $\sqrt{3}$ and $\sqrt{19}$, respectively. Neglecting the $2CO + O_2 \rightleftharpoons 2CO_2$ equilibrium, the chemical potentials of CO and O, $\mu_{CO}(T, p_{CO}) = E_{CO}^{total} + \Delta\mu_{CO}(T, p_{CO})$ and $\mu_O(T, p_{O_2}) = 1/2E_{O_2}^{total} + \Delta\mu_O(T, p_{O_2})$, become independent variables [26]. The E^{total}'s are the total electronic energies of the gas phase molecules. The $\Delta\mu$'s are tabulated in [26]. At for instance $T = 300, 400, 500$ K, $p_{CO} = p_{O_2} = 1$ atm, we have $\Delta\mu_{CO} = -0.53, -0.73, -0.95$ eV and $\Delta\mu_O = -0.27, -0.38, -0.50$ eV.

the Pt surface. This structure is the well-characterized low-pressure, room-temperature equilibrium structure [5] of CO at Pt(111). The GGA-PW91 based phase diagram depicted in Fig. 2b shows all phases shifted to lower chemical potentials as a consequence of

the stronger adsorbate binding [10] with this XC functional, which means that the CO saturation phase, $(\sqrt{19} \times \sqrt{19})R23.4° - 13CO$ [27,28], is predicted to occur even at the relatively high temperatures of interest here. Staying consistent with the use of the GGA-RPBE functional, we choose, however, to adapt the $c(4 \times 2)$-2CO structure far from the oxide edge. Right at the oxide edge, we further include the possibility of a higher (local) CO coverage. A number of different relative registries of the CO overlayer to the PtO$_2$ ad-structure has been considered as shown in Fig. 1, structures A1–B2. We anticipate that including even more variation in the oxide and CO domain orientations and registries would lead to the discovery of more special sites. However, to keep the study tractable, we settle on the present set which is already large enough to demonstrate our point.

Table 1 summarizes the energetics of the CO binding at the metallic Pt(111) in front of an α-PtO$_2$ patch. Far from the oxide edge, the ordinary $c(4 \times 2)$-2CO overlayer sites are filled with CO binding with approximately 1.4 eV until the sites right in front of the oxide edge are reached. Depending now on the registry of the $c(4 \times 2)$-2CO overlayer to the oxide, CO here binds: (i) in ordinary $c(4 \times 2)$ sites (case A1, B2), (ii) in new sites without distorting preadsorbed CO (case A2, A4), or in new sites created by distorting preadsorbed CO (case B1, A3). The CO binding strength is typically reduced in the sites close to the oxide and sites binding CO with less than 0.59 eV (corresponding to μ_{CO} at 330 K and 1 atm pressure) have been omitted since such sites will show little occupation at the temperatures and pressures of interest for catalysis.

For comparison, we include in Fig. 1 the geometry of the known $p(2 \times 2)$-(O + CO) coadsorption structure and of a possible $c(4 \times 2)$-2CO/$p(2 \times 2)$-(O + CO) phase boundary. The differential CO adsorption potential energy is −1.16 eV for CO(3) at the phase boundary, Fig. 1D, which is less than the −1.46 and −1.32 eV calculated for CO inside the $c(4 \times 2)$-2CO and $p(2 \times 2)$-(O + CO) structures, respectively.

Table 1
Calculated GGA-RPBE(GGA-PW91) adsorption potential energies (in eV) for sequential adsorption of CO molecules, i.e., the reaction energies for the N–CO$_a$ + CO$_g$ → $(N + 1)$–CO$_a$ reactions

N	3	4	5	6
A1	−1.45 (−1.86)	−1.08 (−1.52)	−1.07 (−1.51)	–
A2	−1.41 (−1.76)	−0.84 (−1.28)	−0.95 (−1.38)	–
A3	–	−1.46 (−1.88)	−1.45 (−1.87)	−1.06 (−1.53)
A4	−1.40 (−1.75)	−0.59 (−1.11)	−0.67 (−1.14)	–
B1	–	−1.34 (−1.82)	−1.28 (−1.77)	−0.97 (−1.41)
B2	–	−1.34 (−1.74)	−1.36 (−1.76)	–

Table 2
Calculated properties for the $CO_g + O_{ox} \rightarrow CO_{2,g}$ reaction

	E_{CO} eV	E_O eV	ΔE eV	E_a eV	d_{TS} Å	θ_{TS} deg
A1	−1.07 (−1.51)	−1.25 (−1.59)	−0.82(−0.20)	0.23(0.22)	1.70	110
A2	−0.95 (−1.38)	−1.32 (−1.66)	−0.94(−0.29)	0.24(0.20)	1.85	106
A3	−1.36 (−1.82)	−1.36 (−1.69)	−0.51(0.14)	0.70(0.68)	1.82	109
A4	−0.67 (−1.14)	−1.36 (−1.68)	−1.26(−0.60)	0.08(0.07)	1.81	109
B1	−1.15 (−1.63)	−0.77 (−1.03)	−0.98(−0.51)	0.61(0.60)	2.10	102
B2	−1.36 (−1.76)	−1.34 (−1.64)	−0.50(0.04)	0.65(0.66)	1.64	113
C	−1.31 (−1.65)	−0.69 (−1.02)	−1.17(−0.64)	0.74(0.76)	2.00	108
D	−1.32 (−1.65)	−0.44 (−0.77)	−1.43(−0.90)	0.53(0.54)	2.00	108

E_{CO} and E_O are the differential CO and O adsorption potential energies in the initial state, respectively. ΔE and E_a are the reaction energy and reaction barrier, respectively. d_{TS} and θ_{TS} are the transition state OC–O bond length and angle, respectively. Energies are calculated using the GGA-RPBE (GGA-PW91) XC functional. The E_{CO} and E_O values evaluated with the GGA-PW91 become about 0.5 and 0.35 eV lower than the values evaluated with the GGA-RPBE. The ΔE's become about 0.6 eV more endothermic in the GGA-PW91, while the E_a's appear almost independent of the XC functional used.

4. Reaction at three-phase boundary

Starting from the phase boundary situations presented in Fig. 1, we have conducted a search for CO oxidation pathways, TSs and energy barriers. The oxygen was taken from the oxide edge, and the various CO molecules in front of the edge were tested. The lowest possible energy barriers are reported in Table 2, where also our values for the barriers at the two reference systems are given. Fig. 3 illustrates the TSs found. Since A1, A2, A3, A4 and B2 have similar TSs, only A1 has been depicted. At the various models of the metal/metal-oxide phase boundary, the lowest energy barriers found are in the range 0.08–0.70 eV. The barriers at three-phase boundaries are thus lower than the barrier for CO oxidation inside the $p(2 \times 2)$-(O + CO) coadsorption phase on Pt(1 1 1), Fig. 1C. For the latter we calculate 0.74 eV in excellent agreement with calculated barriers of 0.75 and 0.8 eV reported by Eichler and Hafner [29] and Liu and Hu [30], respectively. The CO oxidation barriers calculated for some of the three-phase boundary models (A1, A2, and A4) are extremely low indicat-

ing that the CO will not thermalize at such oxide edges but react immediately. We note that the question of which (if any) of the gas/metal/metal-oxide three-phase boundaries exists can only be addressed by considering the reaction kinetics, which is outside the scope of this work. Once CO has reacted with oxygen, O_{ox}, from the oxide, the O_{ox} must be replenished. Judging from the calculated strong differential oxygen binding at the oxide edge we anticipate that this replenishment will be facile either via direct O_2 dissociation or possibly via a $CO_a \cdot O_{2,ox} \rightarrow CO_{2,g} + O_{ox}$ reaction mechanism as reported on rutile $PtO_2(1 1 0)$ [31].

Our finding of the possibility of very low CO oxidation barriers (0.08–0.24 eV) suggests that gas/metal/metal-oxide three-phase boundaries might even be more reactive than the boundaries investigated experimentally by Wintterlin et al. [14] and Kinne et al. [15]. In their work, the boundary between (the gas phase and) two different chemisorption phases over metallic Pt was investigated at temperatures between 237 K and room temperature and energy barriers were determined to 0.49 eV [14] and 0.53 eV [15], respectively.
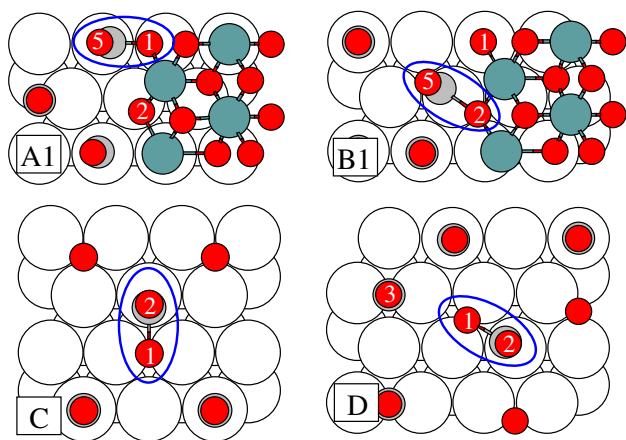

Fig. 3. Transition state geometries for configurations A1, B1, C and D.
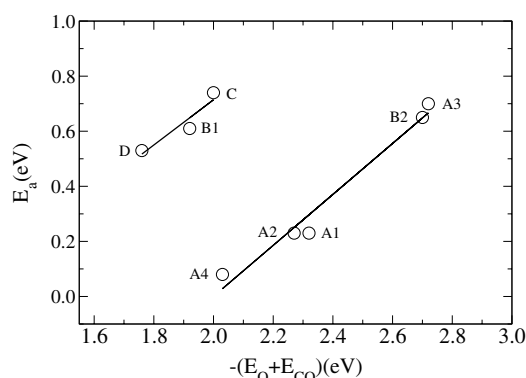

Fig. 4. The calculated energy barrier vs. a measure of the binding energy of the reactants in the initial state, calculated as minus the sum of the individual differential adsorption potential energies of the reacting CO_a and O_{ox}.

Modeling their $c(4 \times 2)$-2CO/$p(2 \times 2)$-(O + CO) phase boundary (Fig. 1D), we calculate an energy barrier of 0.53 eV in good agreement with the experimental values.

In order to trace the origin of the reduced CO oxidation barriers at the three-phase boundary models, we plot in Fig. 4 the energy barrier as a function of the sum of the differential binding energies of the two reactants. The database of minimal reaction energy barriers has been split in two, according to the geometry of the TSs. The points in the lower curve apply to paths in which the CO_a approaches the O_{ox} from a Pt top site via a Pt–Pt bridge site. The points in the upper curve apply to TSs where the CO goes from a Pt top site over a Pt hcp site towards the O_{ox}. The correlation of the stability of an initial state to the energy barrier, which is evident from the figure, is a manifestation of the Brønsted principle [32–34].

Within each set of TSs in Fig. 4, the initial binding energy of the reactants is seen to be the important parameter determining the barrier height. It can thus be concluded that among TSs in the lower curve it is the extraordinary low CO binding in configurations A1, A2, and A4 that cause the vanishing small barriers for these models. However, it can also be seen that owing to the strong binding of the oxygen at the oxide island edge, the overall reactant binding energy (the *x*-coordinate) is larger than in the upper curve. The vertical offset of the two curves is a measure of the intrinsic stability difference of the two transition states. This means that it is mainly the availability of the new, favorable TS [Fig. 3, structure A1] that causes high reactivity of most of the gas/metal/metal-oxide phase-boundary models. It further rationalizes why – somewhat counter-intuitively – it is the O(1) atom in the oxide that reacts rather than O(2) or O(3) that are about 0.25 eV less strongly bound. Neither one of O(2) and O(3) can be approached by CO moving from a Pt top via a Pt–Pt bridge site. That such local environment differences apparently matter significantly demonstrates a high degree of directionality in the Pt–adsorbate bonds [35].

5. Conclusion and outlook

In conclusion, we have investigated with DFT how new special sites might occur at gas/metal/metal-oxide three-phase boundaries. The sites provide favorable reaction pathways with a transition state geometry unlike any other known for gas/metal or gas/metal-oxide two-phase boundaries for the Pt system considered. Due to their higher activity, such special sites might completely dominate the activity of the more abundant two-phase 'normal sites'. In terms of developing more efficient catalysts a viable path may thus be deliberately

to stabilize the three-phase boundaries. In the present work, the same metal was used in the metal surface as in the metal-oxide particle, and the presence of the three-phase boundaries was argued to be controlled by the reaction kinetics. With an alloy-based catalyst, $M_X N_{1-X}$ (e.g., M = Pt, N = Rh), the occurrence of some gas/metallic-$M_Y N_{1-Y}$/oxidized-N three-phase boundary might, however, be controlled by the thermodynamics of the system. Creating special sites at three-phase boundaries in such systems might thus be more easily realizable and thus represents a promising research direction.

References

[1] L. Österlund, P.B. Rasmussen, P. Thostrup, E. Lægsgaard, I. Stensgaard, F. Besenbacher, Phys. Rev. Lett. 86 (2001) 460.
[2] B.L.M. Hendriksen, J.W.M. Frenken, Phys. Rev. Lett. 89 (2002) 046101.
[3] B.S. Clausen, H. Topsøe, Catal. Today 9 (1991) 189.
[4] X.C. Su, P.S. Cremer, Y.R. Shen, G.A. Somorjai, Phys. Rev. Lett. 77 (1996) 3858.
[5] G. Rupprechter, T. Dellwig, H. Unterhalt, H.J. Freund, J. Phys. Chem. B 105 (2001) 3797.
[6] P.L. Hansen, J.B. Wagner, S. Helveg, J.R. Rostrup-Nielsen, B.S. Clausen, H. Topsøe, Science 295 (2002) 2053.
[7] H. Over, Y.D. Kim, A.P. Seitsonen, S. Wendt, E. Lundgren, M. Schmid, P. Varga, A. Morgante, G. Ertl, Science 287 (2000) 1474.
[8] K. Reuter, D. Frenkel, M. Scheffler, Phys. Rev. Lett. 93 (2004) 116105.
[9] R. Imbihl, G. Ertl, Chem. Rev. 95 (1995) 697.
[10] B. Hammer, L.B. Hansen, J.K. Nørskov, Phys. Rev. B 59 (1999) 7413.
[11] J.P. Perdew, J.A. Chevary, S.H. Vosko, K.A. Jackson, M.R. Pederson, D.J. Singh, C. Fiolhais, Phys. Rev. B 46 (1992) 6671.
[12] B. Hammer, K.W. Jacobsen, J.K. Nørskov, Phys. Rev. Lett. 69 (1992) 1971.
[13] A. Alavi, P.J. Hu, T. Deutsch, P.L. Silvestrelli, J. Hutter, Phys. Rev. Lett. 80 (1998) 3650.
[14] J. Wintterlin, S. Völkening, T.V.W. Janssens, T. Zambelli, G. Ertl, Science 278 (1997) 1931.
[15] M. Kinne, T. Fuhrmann, J.F. Zhu, C.M. Whelan, R. Denecke, H.-P. Steinrück, J. Chem. Phys. 120 (2004) 7113.
[16] D.J. Burnett, A. Capitano, A.M. Gabelnick, A.L. Marsh, D.A. Fischer, John L. Gland, Surf. Sci. 564 (2004) 29.
[17] W.X. Li, L. Österlund, E.K. Vestergaard, R.T. Vang, J. Matthiesen, T.M. Pedersen, E. Lægsgaard, B. Hammer, F. Besenbacher, Phys. Rev. Lett. 93 (2004) 146104.
[18] J. Gustafson, A. Mikkelsen, M. Borg, E. Lundgren, L. Köhler, G. Kresse, M. Schmid, P. Varga, J. Yuhara, X. Torrelles, C. Quirós, J.N. Andersen, Phys. Rev. Lett. 92 (2004) 126102.
[19] C. Soulard, X. Rocquefelte, S. Jobic, D. Dai, H.-J. Koo, M.-H. Whangbo, J. Solid State Chem. 175 (2003) 353.

[20] W.H. Weber, G.W. Graham, J.R. McBride, Phys. Rev. B 42 (1990) 10969.

[21] N.A. Saliba, Y.L. Tsai, C. Panja, B.E. Koel, Surf. Sci. 419 (1999) 79.

[22] C.R. Parkinson, M. Walker, C.F. McConville, Surf. Sci. 545 (2003) 19.

[23] P.A. Carlsson, L. Österlund, P. Thormählen, A. Palmqvist, E. Fridell, J. Jansson, M. Skoglundh, J. Catal. 226 (2004) 422.

[24] M. Ackermann, B.L.M. Hendriksen, J.W.M. Frenken, et al. (to be published).

[25] T.M. Pedersen, W.X. Li, B. Hammer (to be published).

[26] K. Reuter, M. Scheffler, Phys. Rev. B 68 (2003) 045407.

[27] E.K. Vestergaard, P. Thostrup, T. An, E. Lægsgaard, I. Stensgaard, B. Hammer, F. Besenbacher, Phys. Rev. Lett. 88 (2002) 259601.

[28] J.C. Davies, R.M. Nielsen, L.B. Thomsen, I. Chorkendorff, A. Logadottir, Z. Lodziana, J.K. Nørskov, W.X. Li, B. Hammer, S.R. Longwitz, J. Schnadt, E.K. Vestergaard, R.T. Vang, F. Besenbacher, Fuel Cells 4 (2004) 309.

[29] A. Eichler, J. Hafner, Phys. Rev. B 59 (1999) 5960.

[30] Z.P. Liu, P. Hu, J. Chem. Phys. 115 (2001) 4977.

[31] X.Q. Gong, R. Raval, P. Hu, Phys. Rev. Lett. 93 (2004) 106104.

[32] Barriers for dissociative adsorption reactions decrease with increasing adsorption binding energies [33], while barriers for associative desorption reactions decrease with decreasing reactant adsorption binding energies [34].

[33] A. Logadottir, T.H. Rod, J.K. Nørskov, B. Hammer, S. Dahl, C.J.H. Jacobsen, J. Catal. 197 (2001) 229.

[34] X.Q. Gong, Z.P. Liu, R. Raval, P. Hu, J. Am. Chem. Soc. 126 (2004) 8.

[35] P.J. Feibelman, Phys. Rev. B 56 (1997) 10532.